Journal of Experimental and Theoretical Physics, Vol. 98, No. 4, 2004, pp. 760–769.
Translated from Zhurnal Éksperimental'noĭ i Teoreticheskoĭ Fiziki, Vol. 125, No. 4, 2004, pp. 868–878.

SOLIDS
Electronic Properties

Short-Range Order, Large-Scale Potential Fluctuations, and Photoluminescence in Amorphous SiN_x

V. A. Gritsenko[a,*], D. V. Gritsenko[a], Yu. N. Novikov[a], R. W. M. Kwok[b], and I. Bello[c]

[a] *Institute of Semiconductor Physics, Siberian Division, Russian Academy of Sciences, Novosibirsk, 630090 Russia*
[b] *Department of Chemistry, Chinese University of Hong Kong, Shatin, Hong Kong, China*
[c] *Department of Physics and Materials Science, City University of Hong Kong, Tat Chee Avenue, Hong Kong, China*
**e-mail: grits@isp.nsc.ru*
Received September 9, 2003

Abstract—The short-range order and electron structure of amorphous silicon nitride SiN_x ($x < 4/3$) have been studied by a combination of methods including high-resolution X-ray photoelectron spectroscopy. Neither random bonding nor random mixture models can adequately describe the structure of this compound. An intermediate model is proposed, which assumes giant potential fluctuations caused by inhomogeneities in the local chemical composition. The characteristic scale of these fluctuations for both electrons and holes is about 1.5 eV. The photoluminescence in SiN_x is interpreted in terms of the optical transitions between quantum states of amorphous silicon clusters. © *2004 MAIK "Nauka/Interperiodica".*

1. INTRODUCTION

Amorphous silicon nitrides SiN_x, together with silicon dioxide SiO_2, are the main dielectrics used in modern silicon-based electronic devices. Silicon nitride exhibits a unique memory effect, being capable of localizing and capturing injected electrons and holes with a giant time of localized carrier trapping (about 10 years at 300 K) [1]. In recent years, the memory effect in silicon nitride has been used for developing electrically re-writeable ROM devices of Giga- and Terabit capacity [2].

There are two alternative models describing the structure of amorphous layers of nonstoichiometric tetrahedral silicon compounds (SiO_x, SiO_xN_y, SiN_x): the random mixture (RM) model and the random bonding (RB) model [3–17]. The RM model assumes that SiN_x comprises a mixture of two phases, amorphous silicon (a-Si) and silicon nitride (Si_3N_4), and is composed of $SiSi_4$ and SiN_4 tetrahedra [8, 10]. According to the RB model, the structure of SiN_x represents a network composed of $SiN_\nu Si_{4-\nu}$ tetrahedra of five types with $\nu = 0$–4 [3, 4, 11, 12]. Since amorphous SiN_x is synthesized under thermodynamically nonequilibrium conditions, the product structure depends on the method of synthesis. In particular, it was established that the structure of SiN_x obtained by plasma deposition is described by the RM model [8]. Silicon-based devices also widely employ SiN_x synthesized by high-temperature pyrolysis of silicon- and nitrogen-containing gas mixtures. The silicon-containing component is typically silane SiH_4, silicon tetrachloride $SiCl_4$, or dichlorosilane SiH_2Cl_2, while the nitrogen-containing gas is ammonium NH_3. The process is carried out at a temperature of 700–800°C. The structure (short-range order) of SiN_x obtained by pyrolysis still remains unstudied.

Although the memory effect in SiN_x has been studied for more than a quarter of century, the nature of traps responsible for the localization of electrons and holes is still unknown [1, 3]. It was suggested [1] that the role of traps for electrons and holes in SiN_x can be played by silicon clusters. Recently, Park *et al.* [17] observed a photoluminescence (PL) from quantum dots in plasma deposited SiN_x. Therefore, we may suggest that amorphous silicon quantum dots can exist in pyrolytic SiN_x as well and can be detected by PL measurements.

This paper reports on the results of investigations into the short-range order, electron structure, and photoluminescence in amorphous SiN_x synthesized by pyrolysis. Based on the structural data, we propose a model assuming large-scale potential fluctuations caused by inhomogeneities of the local chemical composition of SiN_x. The photoluminescence observed in SiN_x ($x \approx 4/3$) is interpreted in terms of the optical transitions between quantum states of amorphous silicon clusters.

2. SAMPLE PREPARATION AND EXPERIMENTAL TECHNIQUES

The experiments were performed with SiN_x samples synthesized in a low-pressure reactor by chemical

1063-7761/04/9804-0760$26.00 © 2004 MAIK "Nauka/Interperiodica"

vapor deposition (CVD) at 760°C from a SiH_2Cl_2–NH_3 gas mixture. The samples of SiN_x with various compositions were obtained by changing the ratio of SiH_2Cl_2 and NH_3 in the gas phase. The SiN_x layers were deposited onto *p*-Si(100) substrates with a resistivity of $\rho \approx 10\ \Omega$ cm. The luminescence was studied in the samples of SiN_x with $x = 4/3$ synthesized by decomposition of a SiH_4–NH_3–H_2 mixture at 890°C.

High-resolution X-ray photoelectron spectroscopy (XPS) measurements were performed in a Kratos AXIS-HS system using a source of monochromated AlK_α X-ray radiation with $\hbar\nu = 1486.6$ eV. The natural oxide film from the samples was removed by 2-min etching in an HF–methanol mixture (1 : 30), followed by rinsing in methanol. Prior to XPS measurements, the samples were washed in cyclohexane and blown with flow of dry nitrogen. The binding energies were measured relative to the 1*s* peak of carbon in cyclohexane with a binding energy of 285.0 eV. In cases of significant positive charging of a sample, the charge was compensated using a beam of low-energy electrons. All the XPS measurements (except for the angle-resolved ones) were performed for the sample surface oriented perpendicularly to the electron energy analyzer axis (zero polar angle).

In order to check that the XPS spectra reflect the bulk properties of SiN_x, we performed angle-resolved measurements on a Phi Quantum 2000 spectrometer. Figure 1 shows the XPS spectra of Si 2*p* levels in $SiN_{0.51}$ measured for the photoelectron take-off angles of 20, 45, and 90°. Weak angular dependence of the signal shape shows evidence that the bulk of a sample is probed, so that the XPS data obtained reflect the bulk properties of SiN_x.

In the study of SiN_x layers with different compositions (i.e., with variable *x*), we have used a nearly soichiometric silicon nitride (Si_3N_4) as a reference sample for determining the relative sensitivity factors with respect to Si 2*p* and N 1*s* photoelectron lines. The reference sample synthesized at 800°C from a $SiCl_4$–NH_3 mixture with a 1 : 10 ratio of components had a refractive index of 1.96 and exhibited a characteristic IR absorption band at 3300 cm^{-1} due to the stretching vibrations of SiN–H bonds. The calculated concentration of N–H bonds in this material was 2.1×10^{21} cm^{-3}. Thus, it was established that the reference sample had a composition of $SiN_{1.41}H_{0.05}$.

The Raman spectra were measured on a Renishaw Ramanscope spectrometer using He–Ne laser radiation ($\lambda = 632.8$ Å). The IR absorption spectra were recorded on a Nicolet 550 spectrometer with a resolution of 4 cm^{-1}.

The PL measurements for SuN_x ($x \approx 4.3$) samples were performed at room temperature. The emission spectra were normalized with respect to the sensitivity of the detection system. The sample film thicknesses determined using a laser ellipsometer was about 800 Å. The PL excitation spectra were measured using a deuterium lamp of the DDS-400 type.

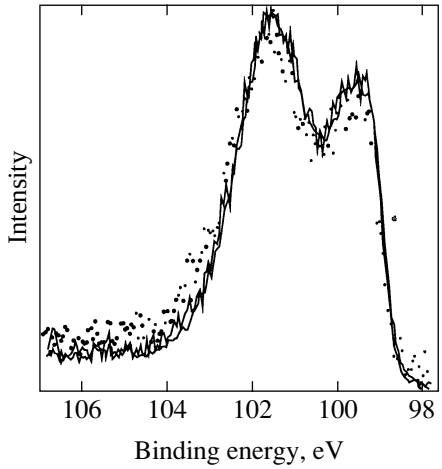

Fig. 1. The XPS spectra of Si 2*p* levels in $SiN_{0.51}$ measured for a photoelectron take-off angle of 20° (points) and 45° and 90° (solid curves).

3. SHORT-RANGE ORDER IN SiN_x BY XPS DATA

Figure 2 shows the experimental XPS spectra (depicted by symbols) of Si 2*p* levels in SiN_x samples of various compositions. All these curves exhibit either two peaks or one peak with a shoulder and are analogous to the spectra reported previously [7, 9, 13]. Applicability of the RB and RM models to description of the structure of SiN_x with variable composition was checked by comparing the experimentally measured Si 2*p* spectra to the results of calculations based on these models.

Dashed curves in Fig. 2 show the XPS spectra calculated in terms of the RB model. This model assumes that the structure consists of $SiN_\nu Si_{4-\nu}$ tetrahedra of five types corresponding to $\nu = 0$–4. The probability to find the tetrahedron with a given ν obeys a binomial distribution [6, 8]

$$W(\nu, x) = \left(\frac{3x}{4}\right)^\nu \left(1 - \frac{3x}{4}\right)^{4-\nu} \frac{4!}{\nu!(4-\nu)!}. \qquad (1)$$

The idea of using five types of tetrahedra for modeling the XPS spectrum of Si 2*p* levels is based on the assumption that only nearest-neighbor silicon and/or nitrogen atoms contribute to the chemical shift of the Si 2*p* electron state. Equation (1) also assumes the absence of point defects such as =N–N= bonds, dangling bonds (≡Si• and =N•), and hydrogen bonds (Si–H, N–H) in SiN_x (here, symbols "–" add "•" denote a covalent bond and an unpaired electron, respectively). The results of electron paramagnetic resonance (EPR)

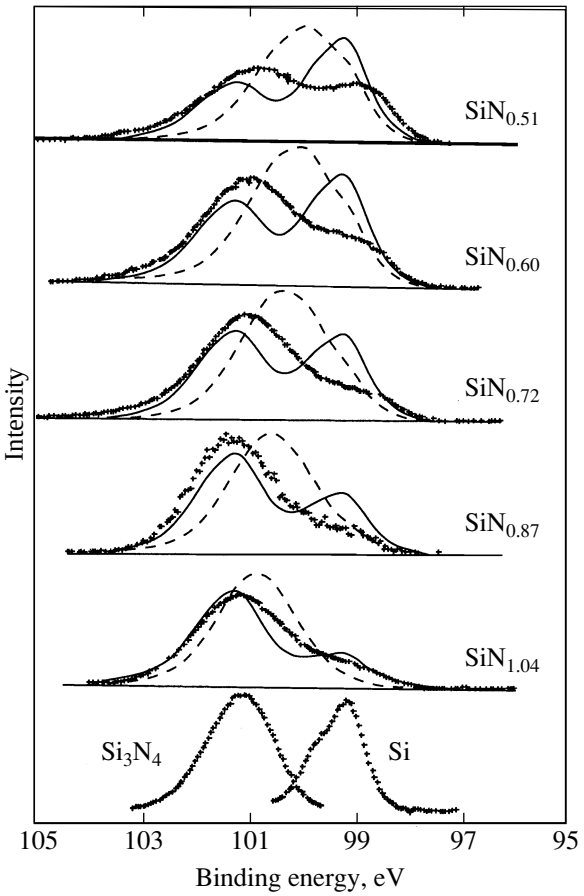

Fig. 2. The XPS spectra of Si 2*p* levels in SiN_x samples of various compositions: symbols represent the experimental spectra; the results of theoretical calculations are depicted by solid (RM model) and dashed (RB model) curves.

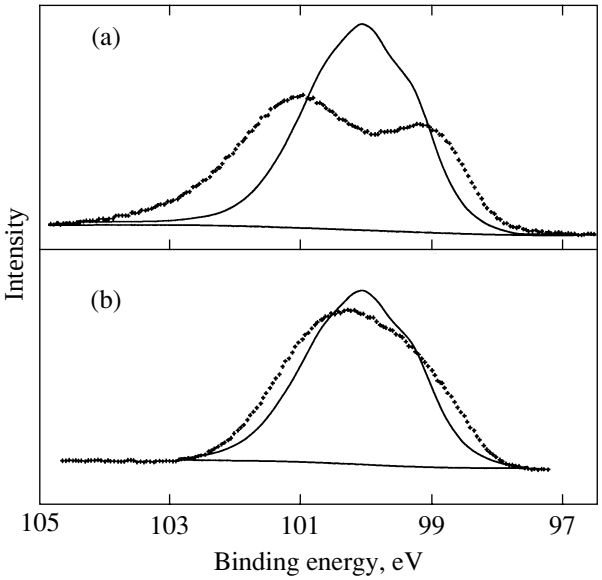

Fig. 3. The XPS spectra (points) of Si 2*p* levels in $SiN_{0.51}$ measured (a) before and (b) after irradiation with 4-keV Ar^+ ions. Solid curves show the results of calculations using the RB model.

measurements showed that the concentration of dangling bonds ≡Si• and =N• in our samples did not exceed 10^{19} cm^{-3}.

Theoretical convolutions of the Si 2*p* spectra were obtained using XPSPEAK 4.1 program package [16]. The theoretical spectra were calculated assuming the peaks corresponding to different SiN_vSi_{4-v} tetrahedra to be equidistant (equally spaced on the energy scale). The peak halfwidth (defined as the full width at half maximum, FWHM) was taken either the same for all peaks or linearly increasing as determined by extrapolation between the peak halfwidth for Si and Si_3N_3. The results of calculations according to the RB model showed that the XPS spectrum of the Si 2*p* level in SiN_x must contain a single maximum (Fig. 2, dashed curves) with the peak position being shifted toward higher binding energies with increasing nitrogen content in SiN_x.

For the sake of generality, we have also checked for the applicability of the RB model to description of the structure of a disordered SiN_x sample. The disorder was produced by irradiating a $SiN_{0.51}$ sample with a beam of 4-keV Ar^+ ions. As can be seen from Fig. 3a, the structure of the initial $SiN_{0.51}$ sample is not adequately described by the RB model: the experimental XPS spectrum exhibits two peaks corresponding (in the first approximation) to the $SiSi_4$ and SiN_4 tetrahedra, whereas the theoretical model predicts a single peak with a maximum positioned at a Si 2*p* binding energy of the SiN_2Si_2 tetrahedron (Fig. 3b). After irradiation, nitrogen and silicon atoms are mixed and the sample exhibits a tendency to form a substitution solid solution (RB model). The XPS spectrum of the ion-bombarded $SiN_{0.51}$ sample displays a single peak with a binding energy of the maximum close to that calculated within the RB model (Fig. 3b).

The results of simulation of the XPS spectra of SiN_x within the framework of the RM model are depicted by solid curves in Fig. 2. The spectra calculated using this model show, in agreement with experiment, a tendency to decrease in the fraction of a silicon phase in SiN_x with decreasing silicon content. However, the RM model somewhat overstates the silicon phase fraction and, in addition, predicts a dip approximately in the middle of the spectrum presented in Fig. 2. In experiments, however, such a dip is observed only for $SiN_{0.51}$ and is absent in the XPS spectra of other samples.

Thus, neither RB nor RM models can quantitatively describe the structure of SiN_x compound. For this reason, we propose an intermediate model illustrated in Fig. 4. This model suggests the presence of separate silicon ($SiSi_4$ tetrahedra) and Si_3N_4 (SiN_4 tetrahedra) phases, as well as subnitrides (composed of SiN_3Si, SiN_2Si_2, and $SiNSi_3$ tetrahedra) in the SiN_x structure. The proposed intermediate model assumes local spatial

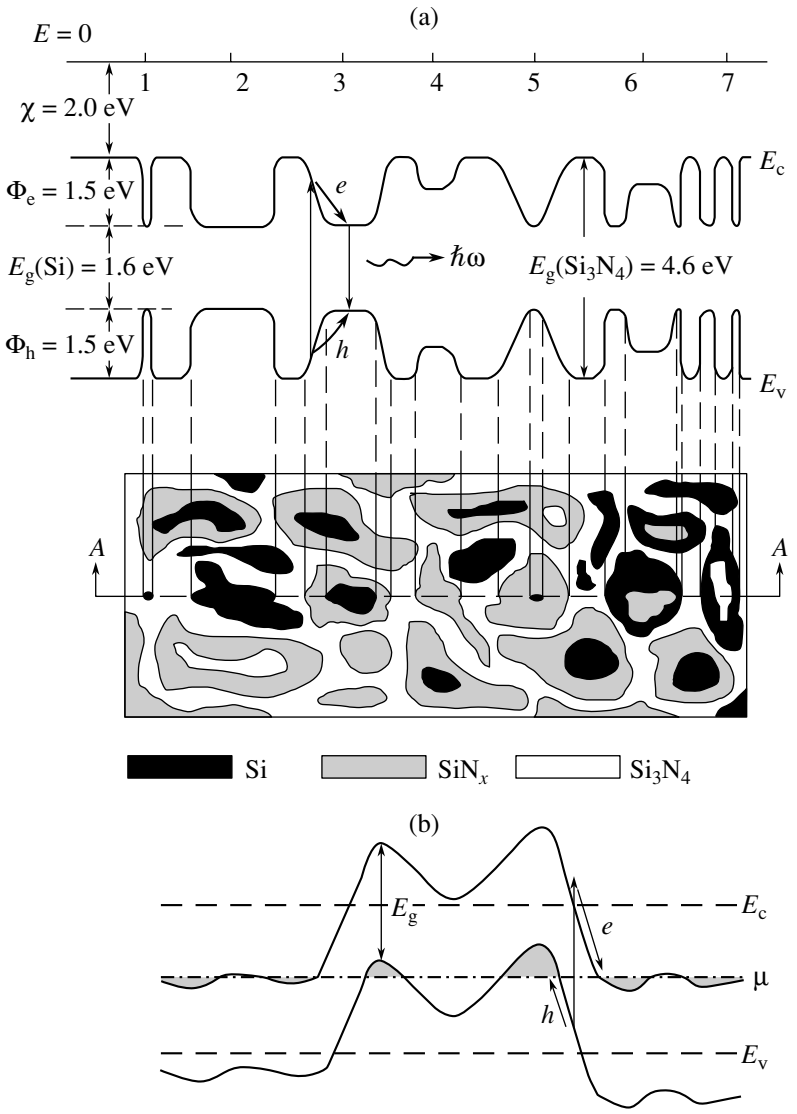

Fig. 4. Schematic diagrams illustrating the proposed intermediate model of SiN_x: (a) a two-dimensional diagram of SiN_x structure showing (bottom) the regions of a silicon phase, stoichiometric silicon nitride, and subnitrides and (top) the energy band profile of SiN_x in the *A*–*A* section (E_c is the conduction band bottom; E_v is the valence band top; Φ_e and Φ_h are the energy barriers for electrons and holes at the a-Si–Si_3N_4 interfaces, respectively; E_g is the bandgap width; and χ is the electron affinity); (b) fluctuations of the Shklovskii–Efros potential in a strongly doped compensated semiconductor (μ is the Fermi level).

fluctuations of the chemical composition of amorphous silicon nitride. This model will be considered in more detail in Section 6.

4. EXCESS SILICON IN SiN_x BY DATA OF RAMAN SCATTERING

The XPS measurements do not provide information on the spatial distribution of silicon in the SiN_x structure. The chemical shift of the Si 2*p* level is sensitive to the local chemical environment, but not to the long-range order. Being nonpolar, Si–Si bonds do not contribute to the IR absorption spectra either. At the same time, the method of Raman scattering allows excess silicon in SiN_x to be detected.

Figure 5 shows the Raman spectra of SiN_x samples of various compositions grown on silicon substrates. Here, an intense peak at 520 cm^{-1} is due to the longitudinal optical phonons in the silicon substrate. For SiN_x samples with a low nitrogen content ($x \le 0.72$), there is an additional weak signal in the region of 460–480 cm^{-1}, that is, at a frequency coinciding with the position of the peak of Raman scattering in amorphous silicon [18]. Previously, the Raman scattering from silicon in SiN_x was studied in [15]. Thus, the Raman spectra pro-

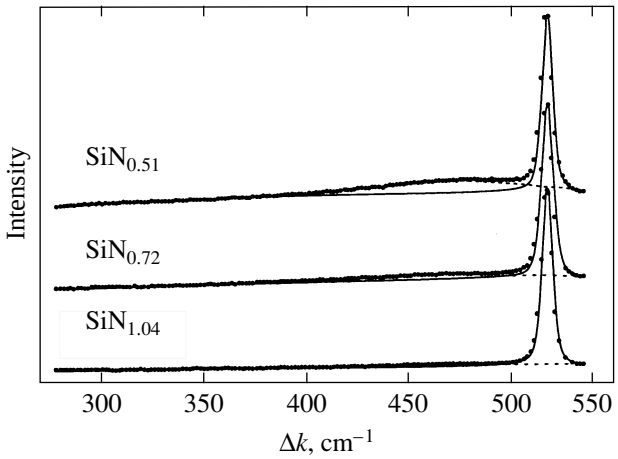

Fig. 5. The Raman spectra of $SiN_{1.04}$, $SiN_{0.72}$, and $SiN_{0.51}$ samples on silicon substrates. The peak at 520 cm^{-1} corresponds to scattering in silicon substrate; the arrow indicates the signal due to scattering from amorphous silicon clusters.

vide an unambiguous evidence of the presence of amorphous silicon clusters in SiN_x.

The bandgap width in Si_3N_4 is $E_g = 4.6$ eV. However, experiments reveal the optical absorption in Si_3N_4 at photon energies below this value [1]. This signal can be attributed to the absorption of light by silicon clusters in a Si_3N_4 matrix. The existence of silicon clusters in SiN_x is also confirmed by data on the fundamental absorption edge, according to which long-wavelength absorption takes place at 1–2 eV [16]. Silicon clusters with dimensions of 12–24 Å in hydrogenated silicon nitride (SiN_x:H) were observed in a high-resolution electron microscope [17, 19]. The Raman spectra of SiN_x with $x \geq 1.04$ exhibit no signal related to the scattering from silicon clusters. However, this result does not exclude the existence of such clusters: the lack of the signal can be explained by insufficient sensitivity of this method, related to small cluster size, low cluster density, and small thicknesses of sample films (about 100 Å).

5. DETERMINING ENERGY BARRIERS FOR HOLES AT THE Si–Si_3N_4 INTERFACE FROM XPS DATA

For a comparative study of the valence bands of Si_3N_4, SiN_x, and a-Si, we have measured the corresponding XPS spectra. The samples of a-Si were prepared by irradiating crystalline silicon with 4-keV Ar^+ ions. The valence band of Si_3N_4 consists of two subbands separated by an ion gap (Fig. 6). The narrow lower subband is formed by N 2*s* orbitals with an admixture of Si 3*s* and 3*p* orbitals [3]. The broad upper subband is formed by the nonbonding $2p_\pi$ orbitals of nitrogen and the bonding 3*s*, 3*p*, and 3*d* orbitals of silicon and 2*p* orbitals of nitrogen [20]. In addition, Fig. 6 presents the high-resolution XPS spectra of Si 3*s*, 3*p*, and 3*d* levels at the valence band top of amorphous $SiN_{1.04}$ measured relative to the valence band top of gold.

As can be seen, features of the valence band spectrum of $SiN_{1.04}$ are generally analogous to those for Si_3N_4, except for the region at the valence band top (Fig. 6b). The high-resolution XPS spectra show that the valence band top of a-Si coincides with that of gold. The electron work function of gold is 5.1 eV. Therefore, the valence band top of a-Si is spaced 5.1 eV from the electron energy level in vacuum. The valence band top of Si_3N_4 is spaced 1.5 eV from the valence band top of a-Si (Fig. 6b). Therefore, the energy barrier for holes at the a-Si–Si_3N_4 interface also amounts to 1.5 eV.

6. LARGE-SCALE POTENTIAL FLUCTUATIONS IN SiN_x CAUSED BY SPATIAL INHOMOGENEITIES OF THE CHEMICAL COMPOSITION

According to the XPS data, SiN_x comprises a mixture of Si_3N_4, silicon subnitrides, and amorphous silicon. The silicon nitride phase is composed of SiN_4 tetrahedra, subnitrides are composed of SiN_3Si, SiN_2Si_2, and $SiNSi_3$ tetrahedra, and the amorphous silicon clusters are composed of $SiSi_4$ tetrahedra. The bandgap width of Si_3N_4 is 4.6 eV, while that of amorphous silicon is 1.6 eV [19, 21] and that of silicon subnitrides varies within 1.6–4.6 eV. Therefore, the bandgap width in SiN_x also varies from 1.6 to 4.6 eV. According to the data presented in Section 5, the maximum scale of potential fluctuations for holes is 1.5 eV. Since the bandgap width of a-Si is 1.6 eV, the energy barrier for electrons at the a-Si–Si_3N_4 interface amounts to 1.5 eV. Thus, the maximum scale of potential fluctuations for electrons in SiN_x is also 1.5 eV.

Figure 4a presents the proposed model of large-scale potential fluctuations caused by variations of the local chemical composition of SiN_x, as illustrated by a two-dimensional diagram showing all possible variants of the local (spatial) structure of silicon nitride. The energy band diagram refers to the *A*–*A* section; the straight line indicates the level from which the electron energies are measured (vacuum level). A decrease in the bandgap width E_g is evidence of the presence of subnitrides in the silicon nitride matrix. The minimum bandgap width ($E_g = 1.6$ eV) corresponds to the silicon phase. This model assumes smooth variation of the chemical composition at the boundaries between silicon clusters and the Si_3N_4 matrix. Our experimental data do not allow the size of this transition region to be estimated. We reckon that this size may be on the order of several dozens of ångströms.

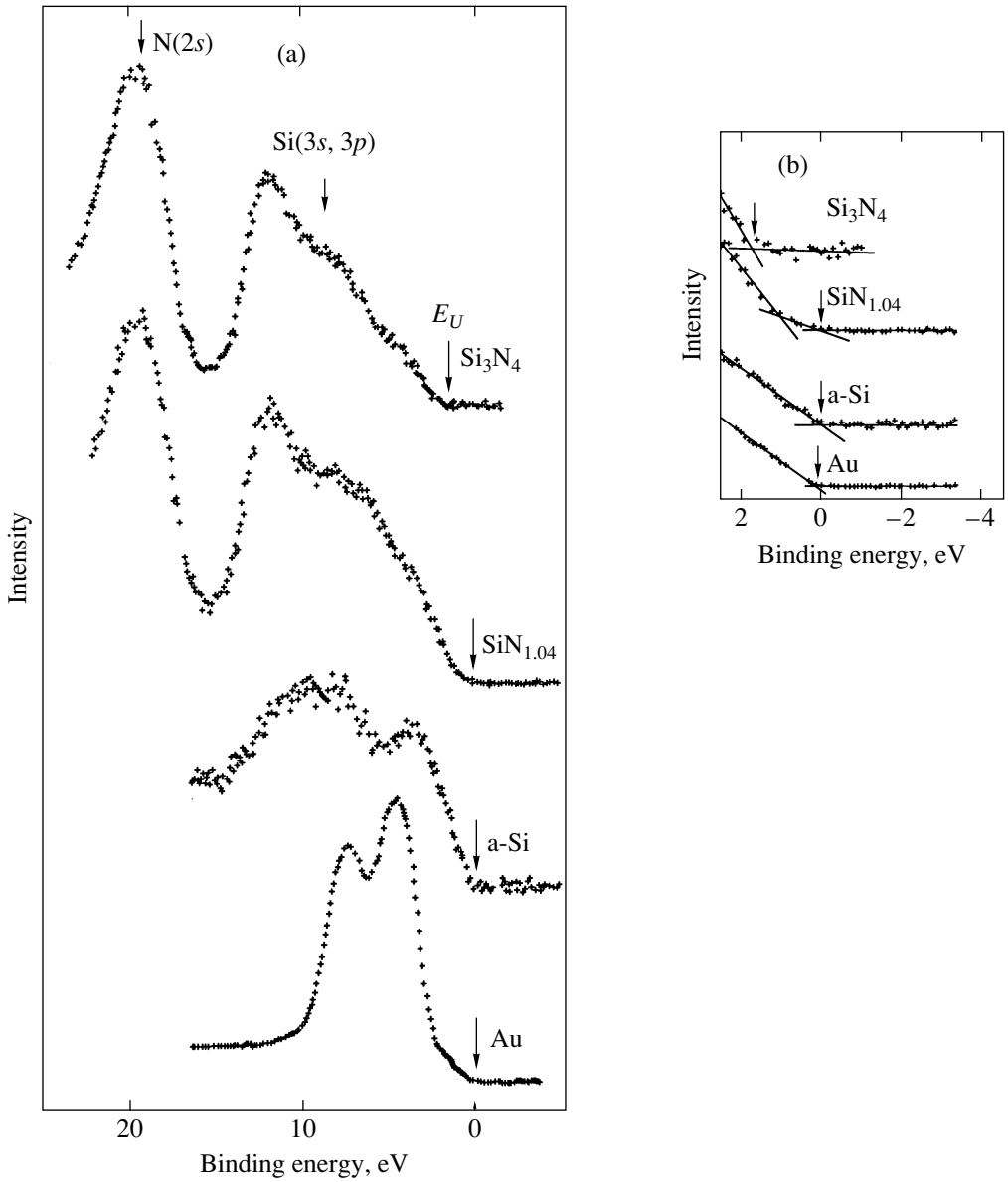

Fig. 6. (a) XPS spectra of the valence band of Si_3N_4, $SiN_{1.04}$, a-Si, and Au (arrows indicate the energy position of the valence band top); (b) the same spectra in the valence band top region recorded at a high resolution.

Region 1 in Fig. 4a corresponds to a "quantum" cluster (with dimensions L on the order of the de Broglie wavelength of quasi-free electrons in a silicon cluster) incorporated into the Si_3N_4 matrix. The ground state energy in this cluster is $E = \hbar^2/2mL^2$, where m is the effective electron mass. Region 2 represents large silicon clusters surrounded by Si_3N_4. In this case, there is no transition layer of subnitrides and the energy band diagram reveals a sharp Si–Si_3N_4 interface. Large clusters do not feature quantization of the energy levels of electrons and holes. Region 3 is a macroscopic silicon cluster surrounded by a silicon subnitride phase. In this situation, the transition from silicon to Si_3N4 in the energy band diagram is smooth. Note that, here and below, we assume that the size of the transition region occupied by silicon subnitrides is significantly greater than the length of Si–N and Si–Si bonds (amounting to 1.72 and 2.35 Å, respectively). Region 4 corresponds to a silicon subnitride cluster in the silicon nitride matrix. Region 5 is a "quantum" silicon cluster incorporated into the subnitride phase, and regions 6 and 7 represent subnitride and nitride clusters, respectively, surrounded by silicon.

Thus, fluctuations of the local chemical composition of SiN_x lead to large-scale spatial fluctuations of the potential for electrons and holes. Previously, similar models of large-scale potential fluctuations have been developed for Si:H [23], SiC:H [24], SiC_xO_z:H [25],

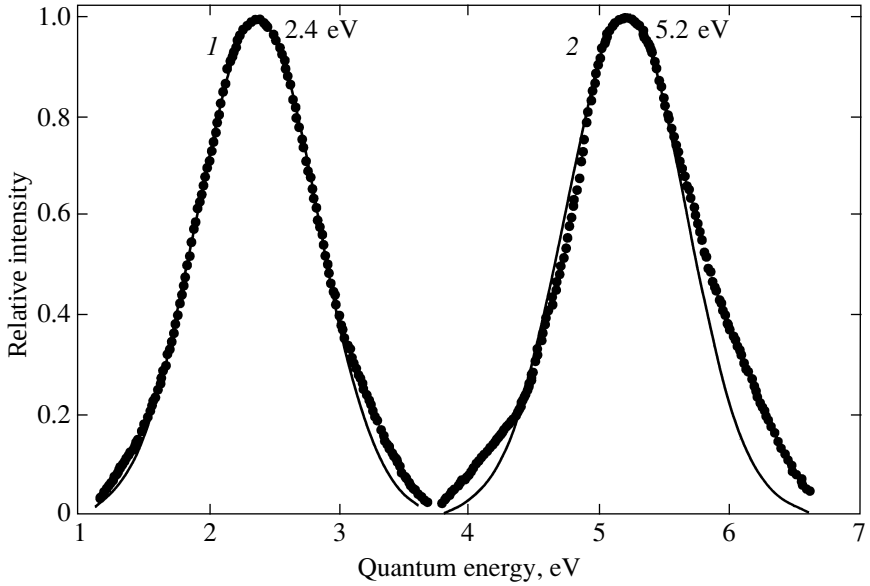

Fig. 7. The spectra of (a) PL and (b) PL excitation in SiN_x ($x \approx 4.3$) at room temperature. Points represent the experimental data, solid curves show the results of approximation by the Gauss function.

and SiO_x [26]. When an electron–hole pair is generated in silicon subnitride, the electric field is directed in the same direction for both electron and hole, thus favoring their recombination (Fig. 6a). In the case of a radiative recombination mechanism, SiN_x is an effective radiative medium. Figure 4b illustrates the Shklovskii–Efros model of large-scale potential fluctuations in a strongly doped compensated semiconductor [2 6]. According to this model, the bandgap width is constant and the potential fluctuations are caused by the inhomogeneous spatial distribution of charged (ionized) donors and acceptors. Here, the electron–hole pair production is accompanied by spatial separation of electrons and holes, thus not favoring their recombination.

7. PHOTOLUMINESCENCE OF SILICON NITRIDE SiN_x

Figure 7 shows the room-temperature PL spectrum of SiN_x ($x \approx 4/3$) with nearly stoichiometric composition excited by quanta with an energy of 5.2 eV (curve *1*). The emission has a maximum intensity at an energy of $E_{lum} = 2.4$ eV. Approximated by a Gauss function, the PL peak has a full width at half maximum (FWHM) of $E_{lum} = 2.4$ eV. The spectrum of excitation of the PL line at 2.4 eV has a maximum at $E_{ex} = 5.2$ eV. The PL excitation spectrum approximated by a Gauss function has the same FWHM (0.92 eV) as that of the emission spectrum. Deviations of the shape of the emission and excitation spectra from the Gauss function are probably caused by experimental errors.

In recent years, the PL spectra of silicon nitride (SiN_x) and oxynitride (SiO_xN_y) of variable compositions have been observed in an energy interval of 2.2–2.8 eV [27–32]. The PL excitation peak at 5.2 eV was reported in [27, 30]. Park *et al.* [17, 19] studied the optical absorption and PL spectra of amorphous silicon clusters in the Si_3N_4 matrix, observed quantum confinement of electrons and holes at these quantum dots, and determined the PL peak energy as a function of the average size of amorphous clusters. As the cluster size decreased from 29 to 13 Å, the PL peak shifted from 1.8 to 2.7 eV. According to [17, Fig. 1], the PL quantum energy of 2.4 eV observed in our experiments corresponds to a silicon cluster size of 17 Å. Figure 8 shows a configuration diagram constructed using the available PL and PL excitation data. The Franck–Condon shift

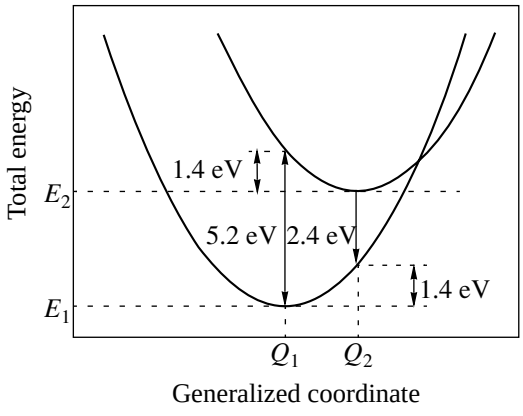

Fig. 8. A configuration diagram of optical transition in a silicon cluster: the lower and upper terms refer to the energies of the ground and excited state, respectively. The optical transitions at 5.2 and 2.4 eV correspond to excitation and emission; 1.4 eV (polaron energy) corresponds to the Franck–Condon shift.

(polaron energy) W_t estimated from this diagram equals to half of the Stokes shift: $W_t = (E_{ex} - E_{lum})/2 = 1.4$ eV.

The width Δ (FWHM) of the PL spectrum is related to the phonon energy W_{ph} in a single-mode approximation as

$$\Delta = 8W_t W_{ph} \ln 2.$$

The phonon energy determined from this relation amounts to $W_{ph} = 109$ eV and the corresponding Hung–Rice ratio is $W_t/W_{ph} = 12.7$. This W_{ph} value is significantly greater than the phonon energy (60 meV) reported for amorphous silicon [33]. The experimentally determined phonon energy coincides with the energy of Si–N bond oscillations in amorphous Si_3N_4 (900 cm^{-1} or 110 meV) [3]. The results can be explained by a large surface to volume ratio for the silicon clusters studied. Thus, the interaction in the excited electron–hole pair is related to local oscillations of the Si–N bonds at the boundary between a silicon cluster and the Si_3N_4 matrix. Previously, a strong interaction in the excited electron–hole pairs in silicon nanoclusters occurring in a SiO_2 matrix was studied by monitoring Si–O oscillations at low temperatures [34, 35]. Thus, according to the proposed interpretation, the emission at 2.4 eV is related to the optical transitions between quantum states of amorphous silicon clusters with an average size of about 17 Å.

8. DISCUSSION OF RESULTS

As was mentioned above, amorphous SiN_x can be synthesized only under thermodynamically nonequilibrium conditions. The structure and properties of this compound depend on the conditions of synthesis (the temperature and gas pressure) and subsequent high-temperature annealing [3]. We have studied the samples of SiN_x prepared at relatively high temperatures. The structure of this material is adequately described by the proposed intermediate model. Ion irradiation of the samples modifies the structure so that it approaches that described by the RB model. When the deposition temperature is decreased (plasma deposition), the structure of the synthesized SiN_x compound is described by the RM model [8].

Previously, it was demonstrated that the intermediate model describes the structure of an amorphous silicon oxide, which is analogous to that of SiN_x and also depends on the conditions of synthesis. In particular, provided that the chemical composition is the same, the optical bandgap width in $SiO_{1.94}$ can be varied from 5.0 to 7.5 eV [36]. Note that the structure of silicon oxynitrides with variable composition SiO_xN_y is quantitatively described (in contrast to the structures of SiN_x and SiO_x) within the framework of the RB model [37, 38].

Basic differences between the proposed model of large-scale potential fluctuations in SiN_x and the Shklovskii–Éfros model for compensated semiconductors are as follows.

(i) Large-scale potential fluctuations in compensated semiconductors are of electrostatic nature, being related to the spatial fluctuations in the density of charged donors and acceptors, while the bandgap width is constant (Fig. 4b). The electric field caused by spatial fluctuations of the potential favors separation of electrons and holes. In SiN_x, the potential fluctuations are caused by inhomogeneities of the local chemical composition. In the proposed intermediate model (Fig. 4a), no space charge is formed (unlike the Shklovskii–Efros model) and the potential fluctuations favor the recombination of electrons and holes.

(ii) The low-frequency dielectric permittivities of Si_3N_4 and Si are 7.0 and 11.8, respectively. Therefore, SiN_x features spatial fluctuations of the permittivity.

(iii) According to the proposed model assuming potential fluctuations in SiN_x, this material is capable of localizing electrons and holes in potential wells, as experimentally observed in [1], with a giant time of localized carrier trapping (about 10 years at 300 K). The proposed intermediate model predicts the possibility of electron and hole percolation in the large-scale potential [25, 26].

The presence of silicon clusters (i.e., regions of significant excess of silicon) in SiN_x is confirmed by Raman scattering data. We believe that the excess silicon is not detected by Raman spectroscopy in nearly stoichiometric silicon nitride (SiN_x with $x \approx 4/3$) because of insufficient sensitivity of this technique. The existence of silicon clusters in SiN_x is confirmed by the following experimental data:

(i) The EPR spectrum of SiN_x displays a signal with $g = 2.0055$ belonging to a Si atom with unpaired electron, bound to three other silicon atoms ($\equiv Si_3Si\bullet$) [39].

(ii) Low-energy electron loss spectrum of SiN_x with $x \approx 4/3$ exhibits peaks at the energies of 3.2 and 5.0 eV, which coincide with the energies of direct electron transitions in silicon [41].

(iii) The fundamental absorption edge in nearly stoichiometric silicon nitride SiN_x ($x \approx 4/3$) is about 4.6 eV [1, 42]. However, experiments on the photothermal absorption [16] showed the presence of absorption in the range from 1.7 to 3.9 eV. This result provides unambiguous evidence of the presence of excess silicon in SiN_x with $x \approx 4/3$.

(iv) The transport of electrons and holes in silicon nitride is conventionally interpreted within the framework of the Frenkel mechanism, according to which the Coulomb potential decreases in a strong electric field [43, 44]. However, our recent results showed that using this model at low temperatures leads to unreasonably small values of the frequency factor ($\nu \approx 10^9$ s^{-1}) and anomalously large tunneling mass of electron ($m^* =$

$5.0m_e$) [45]. It was shown that the charge transfer in silicon nitride in a broad range of temperatures and fields can be quantitatively described using the theory of multiphonon ionization [45].

The thermal energy of trap ionization amounts to 1.4 eV [46], which coincides with the value of the Franck–Condon shift estimated in this study. The energy of local oscillations (60 meV) determined in [46] corresponds to the frequency of oscillations of silicon atoms in silicon clusters. These data provide independent evidence that amorphous silicon clusters act as traps for electrons and holes in silicon nitride.

Nevertheless, this study does not provide a straightforward proof of the existence of silicon clusters with dimensions below 17 Å in nearly stoichiometric SiN_x with $x \approx 4/3$. Previously [47, 48], we formulated a hypothesis that the role of traps in silicon nitride can be played by silicon clusters of minimal size, namely, by Si–Si bonds. Indeed, Gee and Kastner [49] observed the PL at 4.4 eV with an excitation energy of 7.6 eV related to transitions on the Si–Si bonds. Our results presented above do not exclude that Si–Si bonds are the centers responsible for the luminescence at 2.4 eV and for the trapping of electrons and holes in silicon nitride. Thus, further investigations are necessary for judging between the models of amorphous silicon clusters and Si–Si bonds.

9. CONCLUSIONS

We have used high-resolution X-ray photoelectron spectroscopy and Raman scattering to study the short-range order in the layers of silicon nitride of variable composition SiN_x enriched with silicon. It has been established that neither random bonding (RB) nor random Si + Si_3N_4 mixture (RM) models can adequately describe the structure of this compound. An intermediate model has been proposed, according to which the SiN_x structure comprises five types of tetrahedral units, but the probability of finding a given tetrahedron type is not described by the RB model. It is suggested that fluctuations in the local chemical composition lead to large-scale potential fluctuations.

The photoluminescence spectra and the photoluminescence excitation spectra of SiN_x have been measured and interpreted in terms of a model assuming optical transitions between quantum states of amorphous silicon clusters. The Franck–condon shift is 1.4 eV, which coincides with the thermal ionization energy of traps in SiN_x with $x = 4/3$. This result shows evidence that either amorphous silicon clusters or Si–Si bonds (minimal silicon clusters) play the role of traps for electron and holes in nearly stoichiometric silicon nitride.

ACKNOWLEDGMENTS

The authors are grateful to V.V. Vasil'ev for kindly providing experimental data on the photoluminescence and fruitful discussions.

This study was supported by the "Integration" Program of the Siberian Division of the Russian Academy of Sciences (project no. 16) and by the Program "Low-Dimensional Quantum Structures" of the Presidium of the Russian Academy of Sciences.

REFERENCES

1. V. A. Gritsenko, in *Silicon Nitride in Electronics*, Ed. by V. I. Belyi *et al.* (Elsevier, Amsterdam, 1988).
2. V. A. Gritsenko, K. A. Nasyrov, Yu. N. Novikov, *et al.*, Solid-State Electron. **47**, 1651 (2003).
3. V. A. Gritsenko, *Atomic and Electronic Structure of Amorphous Dielectrics in Silicon Based MIS Devices* (Nauka, Novosibirsk, 1993).
4. R. Karcher, L. Ley, and R. L. Johnson, Phys. Rev. B **30**, 1896 (1984).
5. W. R. Knolle and J. W. Osenbach, J. Appl. Phys. **58**, 1248 (1985).
6. V. P. Bolotin, I. A. Brytov, V. A. Gritsenko, *et al.*, Dokl. Akad. Nauk SSSR **310**, 114 (1990).
7. E. Bustarret, M. Bensouda, M. C. Habrard, *et al.*, Phys. Rev. B **38**, 8171 (1988).
8. S. Hasegawa, L. He, T. Inokuma, and Y. Kurata, Phys. Rev. B **46**, 12478 (1992).
9. L. Kubler, R. Haung, E. K. Hill, *et al.*, J. Vac. Sci. Technol. A **4**, 2323 (1986).
10. G. Wiech and A. Simunek, Phys. Rev. B **49**, 5398 (1994).
11. H. R. Philipp, J. Non-Cryst. Solids **8**–**10**, 627 (1972).
12. Z. Yin and F. W. Smith, Phys. Rev. B **42**, 3658 (1990).
13. G. M. Ingo, N. Zacchetti, D. Della Sala, and C. Coluzza, J. Vac. Sci. Technol. A **7**, 3048 (1989).
14. XPSPEAK 4.1, www.ukesca.org, www.phy/cuhk.edu.hksurface.
15. V. A. Volodin, M. D. Efremov, and V. A. Gritsenko, Appl. Phys. Lett. **73**, 1212 (1998).
16. C. H. Seager and J. A. Knapp, Appl. Phys. Lett. **45**, 1060 (1984).
17. N.-M. Park, T.-S. Kim, and S.-J. Park, Appl. Phys. Lett. **78**, 2575 (2001).
18. F. Giorgis, Appl. Phys. Lett. **77**, 522 (2000).
19. N.-M. Park, C.-J. Choi, T.-Y. Seong, and S.-J. Park, Phys. Rev. Lett. **86**, 1355 (2001).
20. V. A. Gritsenko, Yu. N. Novikov, A. V. Shaposhnikov, and Yu. N. Morokov, Fiz. Tekh. Poluprovodn. (St. Petersburg) **35**, 1041 (2001) [Semiconductors **35**, 997 (2001)].
21. D. J. Lockwood, Z. H. Lu, and J.-M. Baribean, Phys. Rev. Lett. **76**, 539 (1996).
22. M. H. Brodsky, Solid State Commun. **36**, 55 (1980).
23. W.-J. Sah, H.-K. Tsai, and S.-C. Lee, Appl. Phys. Lett. **54**, 617 (1989).
24. R. Martins, G. Willeke, E. Fortunato, *et al.*, J. Non-Cryst. Solids **114**, 486 (1989).

25. V. A. Gritsenko, Yu. P. Kostikov, and N. A. Romanov, Pis'ma Zh. Éksp. Teor. Fiz. **34**, 3 (1981) [JETP Lett. **34**, 1 (1981)].
26. B. I. Shklovskiĭ and A. L. Éfros, *Electronic Properties of Doped Semiconductors* (Nauka, Moscow, 1979; Springer, New York, 1984).
2 27. V. V. Vasilev, I. P. Mikhailovskii, and K. K. Svitashev, Phys. Status Solidi A **95**, K37 (1986).
28. K. J. Price, L. E. McNeil, A. Suvkanov, *et al.*, J. Appl. Phys. **86**, 2628 (1999).
29. K. S. Seol, T. Futami, T. Watanabe, *et al.*, J. Appl. Phys. **85**, 6746 (1999).
30. K. S. Seol, Phys. Rev. B **62**, 1532 (2000).
31. T. Noma, K. S. Seol, M. Fujimaki, *et al.*, J. Appl. Phys. **39**, 6587 (2000).
32. H. Kato, N. Kashio, Y. Ohki, *et al.*, J. Appl. Phys. **93**, 239 (2003).
33. F. Giorgis, C. Vinegoni, and L. Pavesi, Phys. Rev. B **61**, 4693 (2000).
34. Y. Kanemitsu, N. Shimitzu, T. Komoda, *et al.*, Phys. Rev. B **54**, 14 329 (1996).
35. Y. Kanemitsu and S. Okamoto, Phys. Rev. B **58**, 9652 (1998).
36. T. W. Hickmott and J. E. Baglin, J. Appl. Phys. **50**, 317 (1979).
37. V. A. Gritsenko, J. B. Xu, R. W. M. Kwok, *et al.*, Phys. Rev. Lett. **81**, 1054 (1998).
38. V. A. Gritsenko, R. W. M. Kwok, H. Wong, and J. B. Xu, J. Non-Cryst. Solids **297**, 96 (2002).
39. Y. Kamigaki, S. Minami, and H. Kato, J. Appl. Phys. **68**, 2211 (1990).
40. R. Hezel and N. Lieske, J. Appl. Phys. **53**, 1671 (1982).
41. P. Y. Yu and M. Cardona, *Fundamentals of Semiconductors* (Springer, Berlin, 1996; Fizmatlit, Moscow, 2001).
42. V. A. Gritsenko, E. E. Meerson, and Yu. N. Morokov, Phys. Rev. B **57**, R2081 (1997).
43. S. M. Sze, *Physics of Semiconductor Devices*, 2nd ed. (Wiley, New York, 1981; Mir, Moscow, 1984).
44. V. A. Gritsenko, E. E. Meerson, I. V. Travkov, and Yu. V. Goltvyanskiĭ, Mikroélektronika **16**, 42 (1987).
45. K. A. Nasyrov, V. A. Gritsenko, M. K. Kim, and H. S. Chae, IEEE Electron Device Lett. **23**, 336 (2002).
46. K. A. Nasyrov, V. A. Gritsenko, and Yu. N. Novikov, Phys. Rev. Lett. (in press).
47. P. A. Pundur, J. G. Shavalgin, and V. A. Gritsenko, Phys. Status Solidi A **94**, k107 (1986).
48. V. A. Gritsenko, H. Wong, I. P. Petrenko, *et al.*, J. Appl. Phys. **86**, 3234 (1999).
49. C. M. Gee and M. Kastner, Phys. Rev. Lett. **42**, 1765 (1979).

Translated by P. Pozdeev

SPELL: 1. re-writeable, Shklovskii—?, 2. Mikhailovskii—?,